2018 European Control Conference (ECC)
June 12-15, 2018. Limassol, Cyprus

Decentralised $\mathcal{L}_1$ Adaptive Controllers for Voltage Control of DC Islanded Microgrids

Daniel O'Keeffe[1], Stefano Riverso[2], Laura Albiol-Tendillo[2], Gordon Lightbody[1,3]

Abstract— **Voltage stability is a critical feature of an efficiently operating power distribution system such as a DC islanded microgrid. Large-scale autonomous power systems can be defined by heterogeneous elements, uncertainty and changing conditions. This paper proposes a novel scalable decentralised control scheme at the primary level of the typical hierarchical control architecture of DC microgrids with arbitrary topology. Local state-feedback $\mathcal{L}_1$ adaptive controllers are retrofitted to existing baseline voltage controllers of DC-DC boost converters, which interface distributed generation units with loads. The use of $\mathcal{L}_1$ adaptive controllers achieves fast and robust microgrid voltage stability in the presence of dynamic uncertainty and plug-and-play operations. Furthermore, local controller synthesis is modular, as at most, it requires approximate information about line parameters that couple neighbouring units.**

I. Introduction

Islanded microgrids (ImGs) have emerged as a Smart Grid initiative to autonomously integrate power-electronic-interfaced distributed generation and storage units (DGU/DSUs) with loads, and provide ancillary services to the utility grid [1]–[4]. The autonomous operation of ImGs relies on the interoperability across electrical, control and communication systems [5]. Key control features of large-scale mGs include; (i) Voltage stability and accurate load-sharing, (ii) Scalability: the ability to design controllers independent of the size and topology of the mG, (iii) Plug-and-play (PnP) operations: the ability to reconfigure DGU/DSUs without compromising global stability conditions, and (iv) Robustness to uncertainty within a heterogeneous system [6], [7].

Voltage stability and accurate load-sharing of the DC-DC power converters that interface DGUs and DSUs with loads is integral to the safe and efficient operation of the ImG. A distributed hierarchical control architecture, utilising classical controllers and low-bandwidth communications, has become the standard within mG research [7], [8]. Though feature (i) is achieved using this approach, (ii)-(iv) are limited [1]–[3]. Stability conditions are only satisfied for specific radial and bus-connected topologies, while homogeneous subsystems are only considered. As identified in [9] and demonstrated in [10], the approach lacks scalability, PnP capabilities and robustness to uncertainty.

*Research is supported by the Irish Research Council enterprise partnership scheme (Award No. R16920) in collaboration with University College Cork, Ireland and United Technologies Research Centre Ireland Ltd.

[1]D. O'Keeffe is with the Control & Intelligent Systems Group at UCC danielokeeffe@umail.ucc.ie. Corresponding author.

[2]S. Riverso and L. Albiol-Tendillo are with UTRC-I Ltd, 4th Floor, Penrose Business Centre, Penrose Wharf, Cork, Ireland.

[1,3]G. Lightbody is with the Control & Intelligent Systems Group and MaREI-SFI Research Centre at UCC.

Recent mG research has addressed features (ii) and (iii). State-of-the-art decentralised PnP controllers have been implemented at the primary layer of the control hierarchy in both DC and AC ImGs of arbitrary topology [9], [11]. These PnP controllers guarantee global asymptotic stability (GAS) by checking the viability of DGU plug-in/out requests through local optimisation problems using linear matrix inequalities. Furthermore, the technique is scalable as local controllers depend only on knowledge of local DGUs and line-couplings. However, the technique is computationally expensive, controller gains are required to discontinuously switch after offline stability checks are performed, and it does not address feature (iv) as robustness to uncertainty is limited.

Due to stakeholder privacy requirements within deregulated energy markets, coupling parameters are generally unknown. Reconfiguration capabilities also lead to *a priori* uncertainty concerning system topology and load information. As a result, robust-adaptive control strategies have become attractive. Existing adaptive strategies applied to primary and secondary control levels [12], [13] use premeditated conditions or linear controllers to provide small-signal adjustments of droop coefficients to achieve global objectives; voltage restoration and load-balancing. Furthermore, these strategies depend on accurate system models, specific mG topologies, and do not address robust adaptation issues, as outlined in [14]. A robust-adaptive control scheme was implemented in [15] but requires an adaptive controller for each global objective, while PnP operations are not facilitated.

This paper proposes a novel scalable decentralised $\mathcal{L}_1$ adaptive control ($\mathcal{L}_1$AC) architecture to ensure fast and robust mG voltage control in the presence of arbitrary topology, PnP operations, unknown interconnections and loads. In a different approach to centralised [16]–[20] and decentralised [21], [22] $\mathcal{L}_1$AC architectures which consider matched interconnections and introduce an additional adaptive law to compensate matched disturbances, the proposed architecture considers unmatched interconnections and provides robustness to unmatched disturbances via baseline controllers with integral action. Furthermore, the architecture ensures GAS by reducing the analysis to providing offline conditions using collective Lyapunov functions.

II. DC Islanded Microgrid Model

A. DGU Quasi Stationary Line Model

For control design objectives, the DC ImG can be modelled as a two-node network [9]. Subsequently, the network is generalised to M-nodes. Each DGU is controlled by

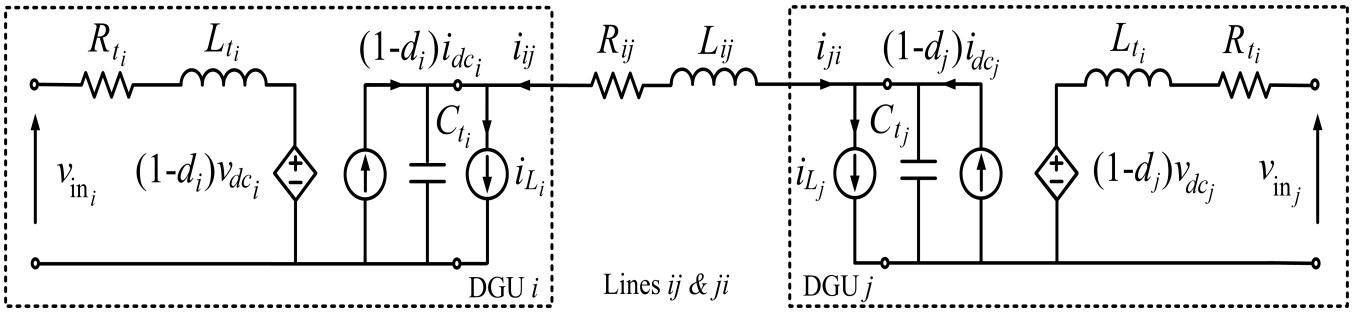

Fig. 1. Averaged nonlinear model of DC ImG composed of two radially coupled boost converter DGUs with unknown loads.

adjusting the duty-cycle d_k ($0 \leq d_k \leq 1$) of a solid-state switch using pulse-width modulation. Fig. 1 represents the averaged dynamics of two boost converters i and j over both on/off switching states. DGUs are coupled via resistive and inductive power lines, for $k \in \{i, j\}$. The ImG is arranged in a general load-connected topology where each DGU supplies power to a local load at the point of common coupling (PCC). Loads are treated as exogenous inputs, which constitute unmatched current disturbances i_{L_k}. This is a positive feature, as the model of each DGU is independent of the load, which can be unknown (e.g. linear resistive, non-linear interfacing buck converters etc.). DGUs can be mapped to a load-connected configuration via the Kron Reduction method [23] which preserves the profile of electrical parameters at the PCC, regardless of topology.

As in [9], Quasi-Stationary Line (QSL) approximations are used to reflect how each DGU is affected by the other.

Assumption 1: Lines ij and ji physically couple each DGU, hence $R_{ij} = R_{ji}$ and $L_{ij} = L_{ji}$. Likewise, in steady-state, $i_{ij} = -i_{ji}$. Furthermore, if the time constant of the line transients is very fast, i.e. L_{ij} and L_{ji} are significantly small, the dynamics of the coupling power lines can be neglected.

Using assumption 1, the line equations are represented in steady-state form i.e. $i_{ij} = \frac{v_{dc_j} - v_{dc_i}}{R_{ij}}$. Applying Kirchoff's voltage and current laws to the DC ImG of Fig. 1, the averaged dynamics of DGU i is represented by:

$$\Sigma^{\text{DGU}}_{[i]} \begin{cases} \dfrac{di_{dc_i}}{dt} = \dfrac{1}{L_{t_i}} v_{\text{in}_i} - \dfrac{(1-d_i)}{L_{t_i}} v_{dc_i} - \dfrac{R_{t_i}}{L_{t_i}} i_{dc_i} \\ \dfrac{dv_{dc_i}}{dt} = \dfrac{(1-d_i)}{C_{t_i}} i_{dc_i} + \dfrac{v_{dc_j}}{R_{ij}C_{t_i}} - \dfrac{v_{dc_i}}{R_{ij}C_{t_i}} - \dfrac{1}{C_{t_i}} i_{L_i} \end{cases} \tag{1}$$

where the states are the inductor current i_{dc_i} and output capacitor voltage v_{dc_i}. Interchanging indexes i and j yields the model for $\Sigma^{\text{DGU}}_{[j]}$.

From (1), the states are multiplied by the control input d_i, thus making the averaged dynamics non-linear. As a result, (1) must be linearised around the operating points $(V_{\text{in}_i}, V_{dc_i}, V_{dc_j}, I_{dc_i}, I_{L_i}, D_i)$ to form a small-signal model[1].

[1]Note: each quantity can be expressed as the sum of its steady-state and small-signal components e.g. $d_k = D_k + \tilde{d}_k$, $v_{dc_k} = V_{dc_k} + \tilde{v}_{dc_k}$ etc.

Written in state-space form, $\Sigma^{\text{DGU}}_{[i]}$ can be represented as,

$$\begin{aligned} \dot{x}_{[i]}(t) &= A_{ii}x_{[i]}(t) + B_i u_{[i]}(t) + E_i w_{[i]}(t) + \zeta_{[i]}(t) + \gamma_{[i]}(t) \\ y_{[i]}(t) &= C_i x_{[i]}(t) \end{aligned} \tag{2}$$

where $x_{[i]} = [\tilde{i}_{dc_i}, \tilde{v}_{dc_i}]^T$ is small-signal state vector, $u_{[i]}(t)$ is the small-signal control input which adjusts the duty-cycle, $w_{[i]}(t) = \tilde{i}_{Li}$ is the small-signal exogenous input, $\zeta_{[i]}(t) = A_{ij}x_{[j]}(t)$ represents coupling with DGU j, and $\gamma_{[i]}(t) = \begin{bmatrix} \frac{1}{L_{t_i}} & 0 \end{bmatrix}^T \tilde{v}_{\text{in}_i}$ is the small-signal input voltage disturbance. The changes in input voltages v_{in_k} are very slow, and thus can be neglected[2]. Therefore $\gamma_i(t) = 0$. The matrices of (2) are,

$$A_{ii} = \begin{bmatrix} -\frac{R_{t_i}}{L_{t_i}} & -\frac{(1-D_i)}{L_{t_i}} \\ \frac{(1-D_i)}{C_{t_i}} & -\frac{1}{R_{ij}C_{t_i}} \end{bmatrix} \; ; \; A_{ij} = \begin{bmatrix} 0 & 0 \\ 0 & \frac{1}{R_{ij}C_{t_i}} \end{bmatrix}$$

$$B_i = \begin{bmatrix} \frac{V_{dc_i}}{L_{t_i}} \\ \frac{-I_{t_i}}{C_{t_i}} \end{bmatrix} \; ; \; E_i = \begin{bmatrix} 0 \\ -\frac{1}{C_{t_i}} \end{bmatrix} \; ; \; C_i = \begin{bmatrix} 0 & 1 \end{bmatrix}$$

where $A_{ii} \in \mathbb{R}^{2\times2}$ is the state matrix; $A_{ij} \in \mathbb{R}^{2\times2}$ is the coupling matrix; $B_i \in \mathbb{R}^2$ is the input vector; $C_i \in \mathbb{R}^{1\times2}$ is the output vector. Furthermore, the steady-state values of the states are given as $V_{dc_i} = \frac{V_{\text{in}_i}}{(1-D_i)}$ and $I_{dc_i} = \frac{V_{\text{in}_i}}{(1-D_i)^2 R_{L_i}}$.

B. ImG Model with M DGUs & Baseline Controller Design

In this section, the two DGU network is generalised to an ImG composed of *M* DGUs. It was demonstrated in [10] that converter coupling dynamics predominantly manifest from physical power lines; duty-cycle coupling is weak. Letting $\mathcal{D} = \{1, ..., M\}$, $\mathcal{M}_i \subset \mathcal{D}$ denotes a neighbour-subset for DGU i. As before, assuming QSL approximation of all line dynamics $(i, j) \in \mathcal{D}$, the DC ImG model is represented by (2), with $\zeta_{[i]}(t) = \sum_{j\in\mathcal{M}_i} A_{ij}x_{[j]}(t)$. The only alteration to (2) is A_{ii} becoming:

$$A_{ii} = \begin{bmatrix} -\frac{R_{t_i}}{L_{t_i}} & -\frac{(1-D_i)}{L_{t_i}} \\ \frac{(1-D_i)}{C_{t_i}} & \sum_{j\in\mathcal{M}_i} -\frac{1}{R_{ij}C_{t_i}} \end{bmatrix} \tag{3}$$

The rationale for implementing an augmentation approach as opposed to a fully adaptive one is that in real systems it

[2]The dynamics of these devices are much slower than the fast switching dynamics of power converters, therefore it is a safe assumption to neglect small-signal changes in input voltage.

is common to have baseline controllers designed to provide reference tracking and disturbance rejection during nominal operation [24]. The idea of this work is to retrofit each DGU, with decentralised $\mathcal{L}_1$ adaptive voltage controllers, in order to enhance the performance of each DGU during operations deviating from the nominal case; parametric uncertainty, PnP operations, unknown load changes. Effectively, the closed-loop DGU can be treated as a black-box. This section details the design of a decentralised static state-feedback (DeSSf) baseline controller.

Remark 1: Though power converter vendors provide details of component values, parametric knowledge of line-couplings, loads, input voltages and hence steady-state duty-cycles are unknown in reconfigurable systems. Moreover, tuning details of baseline controllers designed by vendors may not be provided. As a result, the $\mathcal{L}_1$ACs are designed to account for such uncertainties within a prescribed set.

DeSSf baseline controllers are designed for standalone decoupled converters, assuming a connection to a linear resistive load. The state-space matrices, where dynamics are dependent on a resistive load rather than coupling parameters, are given in [25].

Remark 2: In order to asymptotically track constant voltage references when $w_{[i]}(t)$ is constant, (2) is augmented with integrators. A necessary condition for this is that there must exist equilibrium states $(x^*_{[i]}, u^*_{[i]})$ which verify (2), the proof of which is found in proposition 1 in [9].

The dynamics are defined as,

$$\xi_{[i]}(t) = \int_0^t (r_{[i]}(t) - y_{[i]}(t))dt = \int_0^t (r_{[i]}(t) - C_i x_{[i]}(t))dt \tag{4}$$

where $r_{[i]}(t) = V^{\text{ref}}_{dc_i} - V_{dc_i}$. The DeSSf control law with integral action becomes,

$$\mathcal{C}_{[i]} : u^{bl}_{[i]}(t) = -K^{bl}_i \bar{x}_{[i]}(t) \tag{5}$$

where $K^{bl}_i = [K^i_i, K^v_i, K^\xi_i] \in \mathbb{R}^{1\times 3}$ is the DeSSf control gain vector. Subsequently, the open-loop model augmented with the integral state $\xi_{[i]}(t)$ becomes third order, hence $\bar{x}_{[i]}(t) = [[x_{[i]}(t)]^T, \xi_{[i]}(t)]^T \in \mathbb{R}^3$ is the augmented open-loop state vector. The state-space model of DGU i can now be defined as,

$$\bar{\Sigma}^{\text{DGU}}_{[i]} : \begin{cases} \dot{\bar{x}}_{[i]}(t) = \bar{A}_{ii}\bar{x}_{[i]}(t) + \bar{B}_i u^{bl}_{[i]}(t) + \bar{E}_i \bar{w}_{[i]}(t) + \bar{\zeta}_{[i]}(t) \\ \bar{y}_{[i]}(t) = \bar{C}_i \bar{x}_{[i]}(t) \end{cases} \tag{6}$$

where $\bar{w}_{[i]} = [w_{[i]}, r_{[i]}]^T \in \mathbb{R}^2$ is the exogenous input vector, which includes load current disturbance and reference voltage, $\bar{\zeta}_{[i]}(t) = \sum_{j\in\mathcal{M}_i} \bar{A}_{ij}\bar{x}_{[j]}(t)$, and $\bar{y}_{[i]}(t)$ is the measurable output. The matrices of (6) are defined as,

$$\bar{A}_{ii} = \begin{bmatrix} A_{ii} & 0_{2\times 1} \\ -C_i & 0 \end{bmatrix} \bar{A}_{ij} = \begin{bmatrix} A_{ij} & 0_{2\times 1} \\ 0_{1\times 2} & 0 \end{bmatrix} \bar{B}_i = \begin{bmatrix} B_i \\ 0 \end{bmatrix}$$
$$\bar{C}_i = \begin{bmatrix} C_i & 0 \end{bmatrix} \bar{E}_i = \begin{bmatrix} E_i & 0_{2\times 1} \\ 0_{1\times 2} & 1 \end{bmatrix}$$

where $\bar{A}_{ii} \in \mathbb{R}^{3\times 3}$, $\bar{B}_i \in \mathbb{R}^{3\times 1}$, $\bar{E}_i \in \mathbb{R}^{3\times 3}$, $\bar{A}_{ij} \in \mathbb{R}^{3\times 3}$ and $\bar{C}_i \in \mathbb{R}^{1\times 3}$.

Assumption 2: Matrices $\bar{A}_{ii}$ and $\bar{B}_i$ have full-rank, and although $\bar{A}_{ii}$ is unknown, $(\bar{A}_{ii}, \bar{B}_i)$ is controllable.

Baseline controllers are generally tuned via pole placement for fast closed-loop performance.

The overall global model of the M DGU ImG can be given by,

$$\bar{\boldsymbol{\Sigma}}^{DGU}_{[M]} : \begin{cases} \dot{\bar{\mathbf{x}}}(t) = \bar{\mathbf{A}}\bar{\mathbf{x}}(t) + \bar{\mathbf{B}}\mathbf{u}(t) + \bar{\mathbf{E}}\bar{\mathbf{w}}(t) \\ \bar{\mathbf{y}}(t) = \bar{\mathbf{C}}\bar{\mathbf{x}}(t) \end{cases} \tag{7}$$

where $\bar{\mathbf{x}} = (\bar{x}_{[1]}, \bar{x}_{[2]}, ..., \bar{x}_{[M]}) \in \mathbb{R}^{3M}, \mathbf{u} = (u_{[1]}, u_{[2]}, ..., u_{[M]}) \in \mathbb{R}^M, \bar{\mathbf{w}} = (\bar{w}_{[1]}, \bar{w}_{[2]}, ..., \bar{w}_{[M]}) \in \mathbb{R}^{2M}, \bar{\mathbf{y}} = (\bar{y}_{[1]}, \bar{y}_{[2]}, ..., \bar{y}_{[N]}) \in \mathbb{R}^M$. Matrices $\bar{\mathbf{A}}$, $\bar{\mathbf{B}}$, $\bar{\mathbf{C}}$ and $\bar{\mathbf{E}}$ are detailed in the section 6.1 of [25]

III. Decentralised $\mathcal{L}_1$ Adaptive Control Design

Conventional MRAC architectures frequently suffer from a trade-off between estimation speed and robustness [14]. Fast estimation/adaptation requires large adaptive gains which can destabilise control-loops. The $\mathcal{L}_1$AC, a modification of the indirect MRAC architecture, decouples this trade-off by inserting a low-pass filter (LPF) at the input to both the plant and state-predictor, as seen in Fig. 2. Consequently, robustness instead depends on the choice of filter-bandwidth, thus enabling fast adaptation [17].

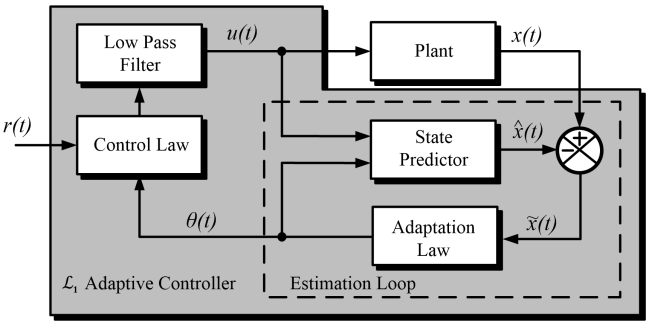

Fig. 2. General Architecture of $\mathcal{L}_1$ Adaptive Controller [17]

Recent criticisms of $\mathcal{L}_1$AC theory have been rebuked in literature and are discussed in [25]. The features of $\mathcal{L}_1$AC have been verified consistently with theory in various safety-critical applications; notably sub-scale NASA aircraft autopilots [18], manned aircraft [26], and unmanned water/aerial vehicles [19], [20]. Moreover, a decentralised $\mathcal{L}_1$AC approach was used to augment aircraft baseline controllers [22]. Typically, these applications use the $\mathcal{L}_1$AC scheme to maintain or recover uniform and predictable performance in the presence of uncertainty or faults, e.g. changes in aerodynamics, loss of control effectiveness [26].

From Fig. 2 a state-predictor replaces the reference model of the indirect MRAC, and a LPF limits the control signal bandwidth. The state-error dynamics between the plant and predictor drives the projection-based adaptation law. This adjusts the control parameters in order to drive $\tilde{x}(t) \to 0$.

A. Plant structure

The plant has a known structure, but with unknown parameter values.

Remark 3: Initially, the unmatched coupling term $\bar{\zeta}_{[i]}$ is neglected to enable local decoupled design. Subsequently, the term is reintroduced in section III.F when GAS conditions are provided.

Remark 4: In [9], disturbance compensators are designed to improve transient performance. However, the design requires subsystems to be minimum phase. Boost converters are non-minimum phase, as analysed in [10]. Using remark 2, the integral action of (5) provides adequate robustness to unmatched disturbances, and therefore $w_{[i]}(t)$ is neglected.

A matched uncertainty term is introduced to represent parametric uncertainty in the dynamics of $\hat{\Sigma}^{\text{DGU}}_{[i]}$, hence (6) can be represented as,

$$\hat{\Sigma}^{\text{DGU}}_{[i]} : \begin{cases} \dot{\bar{x}}_{[i]}(t) = \bar{A}_{ii}\bar{x}_{[i]}(t) + \hat{B}_i(u_{[i]}(t) + \bar{\theta}^T_{[i]}(t)\bar{x}_{[i]}(t)) \\ +Fr_{[i]}(t) \quad ; \quad \bar{y}_{[i]}(t) = \bar{C}_i\bar{x}_{[i]}(t) \end{cases} \tag{8}$$

where $\bar{x}_{[i]}(t) \in \mathbb{R}^3$, is the system measurable state vector; $u_{[i]}(t) \in \mathbb{R}$ is the control signal; $F = \begin{bmatrix} 0 & 0 & 1 \end{bmatrix}^T$; $\bar{\theta}_{[i]}(t) \in \Theta \subset \mathbb{R}^3$ is the unknown parametric uncertainty vector, which belongs to the known uniformly bounded convex set Θ.

B. Control Law

The control input $u(t)$ for $\hat{\Sigma}^{\text{DGU}}_{[i]}$ consists of the summation between the baseline and $\mathcal{L}_1$AC control signals,

$$\mathcal{C}^{\mathcal{L}_1}_{[i]} : u_{[i]}(t) = u^{bl}_{[i]}(t) + u^{\mathcal{L}_1}_{[i]}(t) \tag{9}$$

The augmenting $\mathcal{L}_1$AC law, fitted with a first-order LPF, is

$$u^{\mathcal{L}_1}_{[i]}(t) = -C(s)[\hat{\theta}^T_{[i]}\bar{x}_{[i]}](t) \tag{10}$$

where $C(s) = \frac{\omega_c}{s+\omega_c}$. The robustness of the $\mathcal{L}_1$AC is dependent on the LPF bandwidth ω_c, as subsequently designed.

C. State-predictor

The state-predictor generates an estimate of the system states. From the perspective of the $\mathcal{L}_1$AC, the baseline dynamics are combined with the open-loop DGU dynamics to form an augmented closed-loop system. Without loss of generality, the predictor formulation is proposed for all DGUs,

$$\mathcal{E}_{[i]} : \begin{cases} \dot{\hat{x}}_{[i]}(t) = \hat{A}_m\hat{x}_{[i]}(t) + \hat{B}_m(u^{\mathcal{L}_1}_{[i]}(t) + \hat{\theta}_{[i]}(t)\bar{x}_{[i]}(t)) \\ +Fr_{[i]}(t) \quad ; \quad \hat{y}_{[i]}(t) = \hat{C}_{[i]}\hat{x}_{[i]}(t) \end{cases} \tag{11}$$

where $\hat{x}_{[i]}(t) \in \mathbb{R}^3$ is the predicted state; $\hat{A}_m \in \mathbb{R}^{3\times3}$ is the Hurwitz design matrix that specifies the desired closed-loop dynamics, defined in section F; $\hat{\theta} \in \mathbb{R}^3$ is the parametric estimation vector.

D. Adaptive Law

The adaptive law generates an estimate of the plant uncertainties. Defining the state-error and parametric estimation error vectors as, $\tilde{x}_{[i]}(t) = \bar{x}_{[i]}(t) - \hat{x}_{[i]}(t)$ and $\tilde{\theta}_{[i]}(t) = \bar{\theta}_{[i]}(t) - \hat{\theta}_{[i]}(t)$, the state-error dynamics, used to drive the adaptive law, can be defined as,

$$\dot{\tilde{x}}_{[i]}(t) = \hat{A}_m\tilde{x}_{[i]}(t) + \hat{B}_m\tilde{\theta}_{[i]}(t)\hat{x}_{[i]}(t) \tag{12}$$

The adaptive law is determined from Lyapunov's second stability method. A quadratic Lyapunov candidate is defined as a function in terms of $\tilde{x}_{[i]}(t)$ and $\tilde{\theta}_{[i]}(t)$.

$$\mathcal{V}_{[i]}(\tilde{x}_{[i]}(t), \tilde{\theta}_{[i]}(t)) = \tilde{x}_{[i]}(t)^T P_i\tilde{x}_{[i]}(t) + \tilde{\theta}_{[i]}(t)^T\Gamma_i^{-1}\tilde{\theta}_{[i]}(t) \tag{13}$$

where, $P_i \in \mathbb{R}^{3\times3}$ is a symmetric matrix, such that $P_i = P_i^T > 0$ is the solution to the algebraic Lyapunov linear inequality $\hat{A}_m^T P_i + P_i\hat{A}_m \leq -Q_i$, for arbitrary $Q_i \in \mathbb{R}^{3\times3}$ where $Q_i = Q_i^T > 0$; $\Gamma_i \in \mathbb{R}^+$ is the adaptive gain. If the time-derivative of (13) is at least negative semi-definite, then (8) is locally stable since the energy along the trajectories of state and estimation errors decreases. Following [17], (13) can be written as,

$$\dot{\mathcal{V}}_{[i]}(\tilde{x}_{[i]}(t), \tilde{\theta}_{[i]}(t)) \leq -\tilde{x}_{[i]}(t)^T Q_i\tilde{x}_{[i]}(t) \leq 0 \tag{14}$$

when the adaptive law is defined as,

$$\dot{\hat{\theta}}_{[i]}(t) \triangleq \Gamma_i\text{Proj}(\hat{\theta}_{[i]}(t), -\bar{x}_{[i]}(t)\tilde{x}^T_{[i]}(t)P_i\hat{B}_m) \tag{15}$$

where the projection operator bounds the parametric uncertainty estimate [27]. From (14), $\tilde{x}_{[i]}(t)$ is also bounded. Furthermore, by invoking Barbalat's Lemma, i.e. the second derivative of (13) is bounded, it follows that $\lim_{t\to\infty} \tilde{x}_{[i]}(t) = 0$.

E. Filter Design

The key feature of the $\mathcal{L}_1$AC is the synthesis of a LPF structure in order to decouple robustness from adaptation. At this point, local asymptotic stability has been ensured during nominal operation and adaptation. Here, stability is further ensured by the insertion of the LPF. A closed-loop reference system is defined, where the uncertainty vector is known i.e. $\bar{\theta}_{[i]}(t) = \bar{\theta}^*_{[i]}$, so that performance and robustness specifications can be set independent of the estimation process. Considering the ideal control input as,

$$u^{\text{ref}}_{[i]}(t) - C(s)\bar{\theta}^T_{[i]}\hat{x}^{\text{ref}}_{[i]}(t) \tag{16}$$

the reference system can be given in the Laplace domain as,

$$\hat{x}^{\text{ref}}_{[i]}(s) = G(s)\bar{\theta}^{*\,T}_{[i]}\hat{x}^{\text{ref}}_{[i]}(s)) + r^0_{[i]}(s) + \hat{x}^0_{[i]}(s) \tag{17}$$

where, $\hat{x}^{\text{ref}}_{[i]} \in \mathbb{R}^3$, is the reference state; $r^0_{[i]}(s) = (s\mathbb{I} - \hat{A}_m)^{-1}Fr_{[i]}(s)$; $x^0_{[i]} = (s\mathbb{I} - \hat{A}_m)^{-1}x^{\text{i.c.}}_{[i]}$, where $x^{\text{i.c.}}_{[i]} \in \mathbb{R}^3$ is the initial state; $\mathbb{I} \in \mathbb{R}^{3\times3}$, is the identity matrix; $G(s) = (1 - C(s))H(s)$, and $H(s) = (s\mathbb{I} - \hat{A}_m)^{-1}\bar{B}_m$ is the desired closed-loop behaviour.

As shown in [17], the $\mathcal{L}_1$-norm is now taken on both sides of (17),

$$||\hat{x}^{\text{ref}}_{[i]}||_{\mathcal{L}_1} = \frac{||r^0_{[i]}||_{\mathcal{L}_\infty} + ||x^0_{[i]}||_{\mathcal{L}_\infty}}{1 - ||G(s)\bar{\theta}^{*\,T}_{[i]}||_{\mathcal{L}_1}} \tag{18}$$

For the reference states to be bounded, the denominator must not be zero. As defined in [17], the worst case adaptation bound is $\theta_{\max} = 4\max_{\theta\in\Theta} ||\bar{\theta}^*_{[i]}||_1$ where $\theta_{\max}$ represents the boundary of projection for estimating the parameters when using the adaptation law (15). Finally, for the reference states to remain bounded, the following $\mathcal{L}_1$-norm condition must be satisfied,

$$\lambda = ||G(s)||_{\mathcal{L}_1}\theta_{\max} < 1 \tag{19}$$

where the degree-of-freedom is ω_c. Inserting the LPF enables the $\mathcal{L}_1$AC to compensate uncertainty within the bandwidth of the control channel and attenuates any high frequency content induced by large adaptive gains.

F. Design Considerations and Global Stability Conditions

The desired closed-loop dynamics in (11) are defined as,

$$\hat{A}_m = \begin{bmatrix} A_m - B_m K_{iv}^{\text{nom}} & B_m K_{\xi}^{\text{nom}} \\ -C_i & 0 \end{bmatrix} \hat{B}_m = \begin{bmatrix} B_m \\ 0 \end{bmatrix} \tag{20}$$

A priori knowledge of the real-time steady-state duty-cycle V_{dc_i} and I_{dc_i} values, baseline controller gains, line resistances and the number of neighbouring DGUs is not known. Therefore, A_m and B_m, use nominal parameters which represent an estimate of where the uncertain dynamics lie within a prescribed set. Refer to [25] for more details about the selection of nominal controller gains $K_{\text{nom}} = [K_i^{\text{nom}}, K_v^{\text{nom}} K_{\xi}^{\text{nom}}] \in \mathbb{R}^3$ using the LQR method, nominal parameters and calculation of the parameter bound $\theta_{\max}$.

The overall system, described in (7), is asymptotically stable if the matrix $\mathbf{P}$ satisfies the Lyapunov inequality equation,

$$\underbrace{\hat{\mathbf{A}}_{\mathbf{m}}^T \mathbf{P} + \mathbf{P}\hat{\mathbf{A}}_{\mathbf{m}}}_{\text{(a)}} + \underbrace{\hat{\mathbf{A}}_{\mathbf{C}}^T \mathbf{P} + \mathbf{P}\hat{\mathbf{A}}_{\mathbf{C}}}_{\text{(b)}} < 0 \tag{21}$$

where $\mathbf{P} = \text{diag}(P_i) \in \mathbb{R}^{3M\times 3M}$; $\hat{\mathbf{A}}_{\mathbf{m}} = \text{diag}(\hat{A}_m) \in \mathbb{R}^{3M\times 3M}$ represents the overall desired dynamics; $\hat{\mathbf{A}}_{\mathbf{C}} = \hat{\mathbf{A}} - \hat{\mathbf{A}}_{\mathbf{m}} \in \mathbb{R}^{3M\times 3M}$ represents the coupling dynamics only. As locally each DGU is designed to be asymptotically stable, the matrices of (a) are negative definite. Therefore, to ensure (21) is obeyed, the control gain vector $\mathbf{K} = \text{diag}(K_{\text{nom}}) \in \mathbb{R}^{3M\times 3M}$ is iteratively tuned until $||(a)|| > ||(b)||$ is satisfied.

The decentralised $\mathcal{L}_1$AC architecture is shown below,

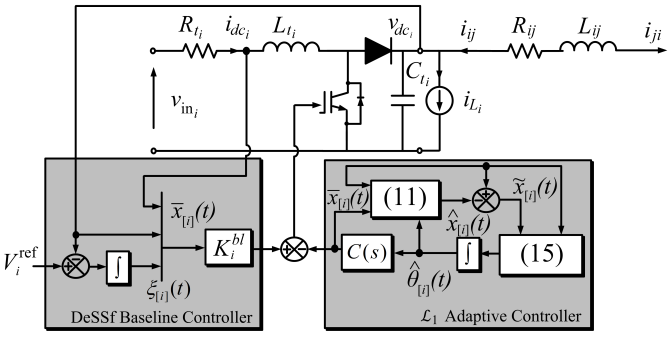

Fig. 3. Primary control level of $\hat{\Sigma}_{[i]}^{\text{DGU}}$ with decentralised $\mathcal{L}_1$AC scheme.

IV. Results

A meshed and radial mG topology, similar to that of [9], is considered in this work. Equipped with only baseline controllers, this system is known to destabilise when $\hat{\Sigma}_{[6]}^{\text{DGU}}$ is plugged-in - see section 6.2 of [25]. Hence, this set-up can adequately evaluate the performance of the proposed decentralised $\mathcal{L}_1$AC augmentation. Each DGU is equipped with controllers $\mathcal{C}_{[i]}^{\mathcal{L}_1}, i = 1, ..., 6$. Simulation of the ImG uses the averaged model of (1) and is perfomed in Matlab/Simulink. System parameters are detailed in Table I of [25]. The dynamics of each DGU are different i.e. the electrical parameters and controller bandwidths are non-identical; therefore, the system can be described as heterogeneous. At $t = 0$ s, $\hat{\Sigma}_{[1]}^{\text{DGU}}, \hat{\Sigma}_{[2]}^{\text{DGU}}, \hat{\Sigma}_{[3]}^{\text{DGU}}$ and $\hat{\Sigma}_{[4]}^{\text{DGU}}$ are connected in a ring configuration. $\hat{\Sigma}_{[5]}^{\text{DGU}}$ is connected to $\hat{\Sigma}_{[4]}^{\text{DGU}}$, while $\hat{\Sigma}_{[6]}^{\text{DGU}}$ powers a local load exclusively.

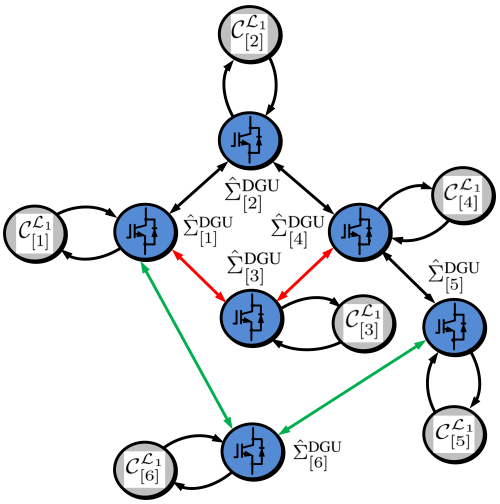

Fig. 4. Meshed and radial microgrid configuration - $\hat{\Sigma}_{[6]}^{\text{DGU}}$ plug-in (green) and $\hat{\Sigma}_{[3]}^{\text{DGU}}$ plug-out (red).

At $t = 2$ s, $\hat{\Sigma}_{[6]}^{\text{DGU}}$ is plugged-in to the network. Fig. 5(a) shows that all responses remain stable and are fast, with the slowest settling time associated with $\hat{\Sigma}_{[6]}^{\text{DGU}}$ at 10 ms. Fig. 5(b) shows $\hat{\Sigma}_{[3]}^{\text{DGU}}$ is plugged-out at $t = 4$ s. Settling times are under 10 ms.

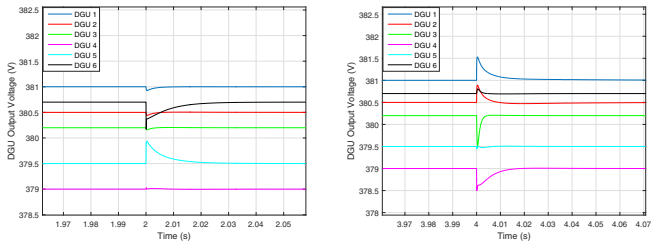

(a) (b)

Fig. 5. (a) DGU voltage responses for $\hat{\Sigma}_{[6]}^{\text{DGU}}$ plug-in and (b) $\hat{\Sigma}_{[3]}^{\text{DGU}}$ plug-out.

Robustness to an unknown load change is evaluated by stepping the load power of $\hat{\Sigma}_{[2]}^{\text{DGU}}$ at $t = 5$ s from 2 kW to 3.8 kW. Fig. 6(a) shows that though undershoot amounts to 2.1 %, settling is achieved within 30 ms. Fig. 6(b) shows the response to $\hat{\Sigma}_{[3]}^{\text{DGU}}$ plugging back in, connecting to $\hat{\Sigma}_{[5]}^{\text{DGU}}$ and $\hat{\Sigma}_{[6]}^{\text{DGU}}$. Again, stability is maintained during PnP operations and responses settle within 10 ms. Primary control references are typically set by secondary controllers that regulate power quality, therefore good tracking is important. Fig. 7 shows a reference step of 379 V - 377 V for $\hat{\Sigma}_{[5]}^{\text{DGU}}$. Tracking is achieved within 25 ms. For more results e.g. the use of nonlinear switching models, controller actuation and robustness to unmodelled dynamics, refer to [25].

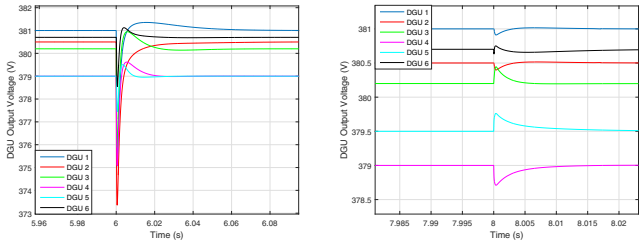

(a) (b)

Fig. 6. (a) DGU voltage responses for $\hat{\Sigma}^{\text{DGU}}_{[2]}$ load step 2 kW-3.8 kW and (b) $\hat{\Sigma}^{\text{DGU}}_{[3]}$ plug-in.

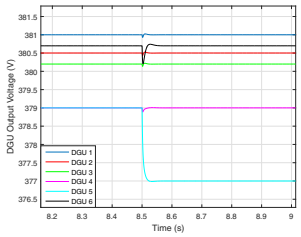

Fig. 7. DGU voltage response for $\hat{\Sigma}^{\text{DGU}}_{[5]}$ reference step of 379 V - 377 V.

V. Conclusion

This paper develops a scalable decentralised $\mathcal{L}_1$AC for augmentation of DGU baseline voltage controllers within a heterogeneous DC ImG of arbitrary topology. These controllers are equipped to DC-DC boost converters at the primary control level and guarantee local asymptotic stability in the presence of parametric and topology uncertainty. Offline conditions for asymptotic stability of the overall mG are also provided. As long as appropriate uncertainty bounds are incorporated, the $\mathcal{L}_1$AC can treat each DGU as a black-box. The control architecture demonstrates very fast output voltage performance when evaluated under PnP operations, unknown load and voltage reference step changes.

Future work will consider bus-connected topologies and the design of distributed $\mathcal{L}_1$AC architectures to systematically guarantee GAS in a scalable PnP fashion.

References

[1] J. M. Guerrero, M. Chandorkar, T. L. Lee, and P. C. Loh, "Advanced control architectures for intelligent microgrids - Part I: Decentralized and hierarchical control," *IEEE Transactions on Industrial Electronics*, vol. 60, no. 4, pp. 1254–1262, 2013.

[2] J. W. Simpson-Porco, F. Dörfler, and F. Bullo, "Synchronization and power sharing for droop-controlled inverters in islanded microgrids," *Automatica*, vol. 49, no. 9, pp. 2603–2611, 2013.

[3] J. Zhao and F. Dörfler, "Distributed control and optimization in dc microgrids," *Automatica*, vol. 61, pp. 18–26, 2015.

[4] D. J. Hogan, M. G. Egan, J. G. Hayes, G. Lightbody, and F. Gonzalez-Espin, "A rapid prototyping tool for load and source emulation in a microgrid test laboratory," *2014 IEEE Applied Power Electronics Conference and Exposition - APEC 2014*, pp. 2245–2252, Mar 2014.

[5] H. Farhangi, "The path of the smart grid," *IEEE Power and Energy Magazine*, vol. 8, no. 1, pp. 18–28, 2010.

[6] M. A. Anuradha and A. Massoud, *IEEE Vision for Smart Grid Controls: 2030 and Beyond: Roadmap*. IEEE CSS, 2013.

[7] L. Meng, Q. Shafiee, G. F. Trecate, H. Karimi, D. Fulwani, X. Lu, and J. M. Guerrero, "Review on Control of DC Microgrids," *IEEE Journal of Emerging and Selected Topics in Power Electronics*, vol. 5, no. 3, pp. 928–948, 2017.

[8] T. Dragicevic, X. Lu, J. C. Vasquez, and J. M. Guerrero, "DC Microgrids - Part I: A Review of Control Strategies and Stabilization Techniques," *IEEE Transactions on Power Electronics*, vol. 31, no. 7, pp. 4876–4891, 2016.

[9] M. Tucci, S. Riverso, J. C. Vasquez, J. M. Guerrero, and G. Ferrari-Trecate, "A Decentralized Scalable Approach to Voltage Control of DC Islanded Microgrids," *IEEE Transactions on Control Systems Technology*, vol. 24, no. 6, pp. 1965–1979, 2016.

[10] D. O'Keeffe, S. Riverso, L. Albiol-Tendillo, and G. Lightbodyt, "Distributed Hierarchical Droop Control of Boost Converters in DC Microgrids," *28th IEEE Irish Signals and Systems Conference*, pp. 1–6, 2017.

[11] S. Riverso, M. Tucci, J. C. Vasquez, J. M. Guerrero, and G. Ferrari-Trecate, "Stabilizing plug-and-play regulators and secondary coordinated control for AC islanded microgrids with bus-connected topology," *Applied Energy*, no. August, pp. 1–21, 2017.

[12] V. Nasirian, S. Moayedi, A. Davoudi, and F. Lewis, "Distributed Cooperative Control of DC Microgrids," *IEEE Transactions on Power Electronics*, vol. 8993, no. c, pp. 1–1, 2014.

[13] T. Dragicevic, J. M. Guerrero, J. C. Vasquez, and D. Skrlec, "Supervisory control of an adaptive-droop regulated DC microgrid with battery management capability," *IEEE Transactions on Power Electronics*, vol. 29, no. 2, pp. 695–706, 2014.

[14] B. D. Anderson, "Failures of adaptive control theory and their resolution," *Communications in Information and Systems*, vol. 5, no. 1, pp. 1–20, 2005.

[15] T. V. Vu, D. Perkins, F. Diaz, D. Gonsoulin, C. S. Edrington, and T. El-Mezyani, "Robust adaptive droop control for DC microgrids," *Electric Power Systems Research*, vol. 146, pp. 95–106, 2017.

[16] C. Cao and N. Hovakimyan, "Design and Analysis of a Novel L1 Adaptive Control Architecture With Guaranteed Transient Performance," *IEEE Transactions on Automatic Control*, vol. 53, no. 2, pp. 3397–3402, 2008.

[17] C. Cao and Hovakimyan, *L1 Adaptive Control Theory: Guaranteed Robustness with Fast Adaptation*. Society for Industrial and Applied Mathematics, 2010.

[18] I. Gregory, E. Xargay, C. Cao, and N. Hovakimyan, "Flight Test of an L1 Adaptive Controller on the NASA AirSTAR Flight Test Vehicle," *AIAA Guidance, Navigation, and Control Conference*, pp. 1–31, 2010.

[19] C. H. Svendsen, N. O. Holck, R. Galeazzi, and M. Blanke, "L1 adaptive manoeuvring control of unmanned high-speed water craft," *IFAC Proceedings Volumes (IFAC-PapersOnline)*, vol. 9, no. PART 1, pp. 144–151, 2012.

[20] B. Michini and J. P. How, "L1 adaptive control for indoor autonomous vehicles: Design process and flight testing," *Proceeding of AIAA Guidance, Navigation, and Control Conference*, no. August, pp. 1–15, 2009.

[21] S. Yoo, C. Cao, and N. Hovakimyan, "Decentralised L1 adaptive control for large-scale non-linear systems with interconnected unmodelled dynamics," *IET Control Theory & Applications*, vol. 4, no. 10, pp. 1972–1988, 2010.

[22] G. Kumaresan and A. Kale, "Application of L1 adaptive controller for the design of a novel decentralized leader follower formation algorithm," *IFAC-PapersOnLine*, vol. 49, no. 1, pp. 706–711, 2016.

[23] F. Dorfler and F. Bullo, "Kron reduction of graphs with applications to electrical networks," *IEEE Transactions on Circuits and Systems I: Regular Papers*, vol. 60, no. 1, pp. 150–163, 2013.

[24] E. Lavretsky and K. A. Wise, *Robust and Adaptive Control with Aerospace Applications*. London: Springer, 2012.

[25] D. O'Keeffe, S. Riverso, L. Albiol-Tendillo, and G. Lightbody, "Voltage Control of DC Islanded Microgrids: Scalable Decentralised L1 Adaptive Controllers," 2018. [Online]. Available: arXiv preprint arXiv:1801.04508

[26] K. A. Ackerman, E. Xargay, R. Choe, N. Hovakimyan, C. M. Cotting, R. B. Jeffrey, M. P. Blackstun, P. T. Fulkerson, T. R. Lau, and S. S. Stephens, "Evaluation of an L1 Adaptive Flight Control Law on Calspans Variable-Stability Learjet," *Journal of Guidance, Control, and Dynamics*, pp. 1–10, 2017.

[27] E. Lavretsky and T. E. Gibson, "Projection Operator in Adaptive Systems," *arXiv preprint, arXiv:1112.4232*, 2011. [Online]. Available: http://arxiv.org/abs/1112.4232